

Effect of many-body interactions on the bulk and interfacial phase behavior of a model colloid-polymer mixture

Marjolein Dijkstra,¹ René van Roij,² Roland Roth,³ and Andrea Fortini¹

¹*Soft Condensed Matter, Debye Institute, Utrecht University, Princetonplein 5, 3584 CC Utrecht, The Netherlands*

²*Institute for Theoretical Physics, Utrecht University, Leuvenlaan 4, 3584 CE Utrecht, The Netherlands*

³*Max-Planck-Institut für Metallforschung, Heisenbergstrasse 3, D-70569 Stuttgart, Germany*
and Institut für Theoretische und Angewandte Physik, Universität Stuttgart, Pfaffenwaldring 57, D-70569 Stuttgart, Germany

(Received 23 November 2005; revised manuscript received 27 February 2006; published 11 April 2006)

We study a model suspension of sterically stabilized colloidal particles and nonadsorbing ideal polymer coils, both in bulk and adsorbed against a planar hard wall. By integrating out the degrees of freedom of the polymer coils, we derive a formal expression for the effective one-component Hamiltonian of the colloids. We employ an efficient Monte Carlo simulation scheme for this mixture based on the *exact* effective colloid Hamiltonian; i.e., it incorporates all many-body interactions. The many-body character of the polymer-mediated effective interactions between the colloids yields bulk phase behavior and adsorption phenomena that differ substantially from those found for pairwise simple fluids. We determine the phase behavior for size ratios $q = \sigma_p / \sigma_c = 1, 0.6,$ and 0.1 , where σ_c and σ_p denote the diameters of the colloids and polymer coils, respectively. For $q = 1$ and 0.6 , we find both a fluid-solid and a stable colloidal gas-liquid transition with an anomalously large bulk liquid regime caused by the many-body interactions. We compare the phase diagrams obtained from simulations with the results of the free-volume approach and with direct simulations of the true binary mixture. Although we did not simulate the polymer coils explicitly, we are able to obtain the three partial structure factors and radial distribution functions. We compare our results with those obtained from density functional theory and the Percus-Yevick approximation. We find good agreement between all results for the structure. We also study the mixture in contact with a single hard wall for $q = 1$. Upon approach of the gas-liquid binodal, we find far from the triple point, three layering transitions in the partial wetting regime.

DOI: [10.1103/PhysRevE.73.041404](https://doi.org/10.1103/PhysRevE.73.041404)

PACS number(s): 82.70.Dd, 64.60.-i, 68.08.-p

I. INTRODUCTION

Mixed suspensions of colloidal spheres and nonadsorbing polymer coils are rich condensed-matter systems, revealing not only fluid-solid coexistence but under the right conditions also fluid-fluid phase coexistence of a colloid-dilute “gas” phase and a colloid-dense “liquid” phase [1–8]. The gas-liquid transition is driven by the depletion effect [1,9], which induces effective attractions between pairs of colloids at surface-surface separations smaller than (about) twice the radius of gyration, R_g , of the polymer; the strength of these attractions increases with the polymer fugacity. A simple model that describes the depletion effect is named after Asakura and Oosawa (AO), and was first formulated by Vrij in 1976 [1]. In the AO model the colloids are treated as hard spheres with diameter σ_c and the interpenetrable polymer coils are treated as noninteracting (ideal) spheres as regards their mutual interactions. The hard core of the colloids, however, excludes the center of mass of a polymeric sphere from the center of a colloid by a distance $\sigma_{cp} \equiv (\sigma_c + \sigma_p)/2$, where we defined the diameter of a polymeric sphere as $\sigma_p = 2R_g$. The bulk phase diagrams of the AO model have been studied extensively over the years—e.g., as a function of the colloid packing fraction η_c and the polymer fugacity z_p at fixed size ratio $q = \sigma_p / \sigma_c$. For $q \leq 0.4$ no stable gas-liquid coexistence was found, regardless the polymer and colloid concentration, while the fluid-solid immiscibility gap broadens considerably with increasing polymer fugacity [10–12]. For sufficiently large polymer sizes, $q > 0.31$ within the perturbation theory

of Ref. [10] or $q > 0.32$ within the free-volume theory of Ref. [11,13], the phase diagram of the AO model does exhibit gas-liquid, liquid-solid, and gas-solid coexistence, with a gas-liquid-solid triple point and a gas-liquid critical point not unlike simple fluids, with z_p playing the role of inverse temperature. Note that these colloidal analogs of simple liquids have an extremely low gas-liquid interfacial tension [14–17], which recently led to the direct experimental observation of capillary waves on the colloidal gas-liquid interface [18].

Even though the AO model is a relatively simple nonadditive hard-sphere mixture [19] it is *not* straightforward to directly simulate it, at least not in all state points and geometries of interest. The main complication is the relatively large number of required (ideal) polymers in the simulation, which causes slow equilibration in the case of, e.g., triple points and wetting of planar walls. In this paper, we circumvent this problem and map the binary mixture onto a one-component system of colloids with polymer-induced effective interactions [20,21], possibly with a many-body character despite the underlying pairwise additive mixture. For size ratios $q < 0.1547$ the effective system is pairwise additive, but otherwise three-body and higher-body terms are not vanishing. We describe a method to perform efficient Monte Carlo simulations for the AO model within this one-component approach and apply it to calculate bulk phase diagrams for size ratios $q = 1, 0.6,$ and 0.1 , as well as structure and adsorption at a planar hard wall for $q = 1$.

The paper is organized as follows. In Sec. II, we describe the model and derive an explicit expression for the effective

one-component Hamiltonian by integrating out the degrees of freedom of the polymer coils formally in the partition function. In Sec. III, we present our efficient Monte Carlo simulation scheme for a model colloid-polymer mixture, which is based on the exact or full effective colloid Hamiltonian. In Sec. IV, we present results of computer simulations based on the exact effective Hamiltonian. Phase diagrams for size ratios $q=1, 0.6$, and 0.1 are shown and compared with those obtained from the free-volume approach. In Sec. V, we present results for the three partial structure factors and pair correlation functions for $q=1$. We compare our results with those obtained from density functional theory and the Percus-Yevick approximation. In Sec. VI, we study the adsorption phenomena of a colloid-polymer mixture in contact with a planar hard wall for $q=1$. Finally, in Sec. VII, we end with some concluding remarks. Parts of this work have been presented elsewhere in a short communication [22,23]. In addition, we refer interested readers to recent topical reviews of colloid-polymer mixtures [21,24] and a detailed review of the statistical mechanics of inhomogeneous model colloid-polymer mixtures [25] and references therein.

II. MODEL AND EFFECTIVE HAMILTONIAN

The interactions in the AO model of N_c colloids at positions \mathbf{R}_i (with $1 \leq i \leq N_c$) and N_p polymers at positions \mathbf{r}_j (with $1 \leq j \leq N_p$) in a macroscopic volume V at temperature T are described by a pairwise colloid-colloid interaction Hamiltonian $H_{cc} = \sum_{i < j}^{N_c} \phi_{cc}(R_{ij})$, a pairwise colloid-polymer Hamiltonian $H_{cp} = \sum_{i=1}^{N_c} \sum_{j=1}^{N_p} \phi_{cp}(|\mathbf{R}_i - \mathbf{r}_j|)$, and a polymer-polymer Hamiltonian $H_{pp} \equiv 0$. Here we introduced the colloid-colloid pair potential ϕ_{cc} and the colloid-polymer pair potential ϕ_{cp} given by

$$\beta\phi_{cc}(R_{ij}) = \begin{cases} \infty & \text{for } R_{ij} < \sigma_c, \\ 0 & \text{otherwise,} \end{cases}$$

$$\beta\phi_{cp}(|\mathbf{R}_i - \mathbf{r}_j|) = \begin{cases} \infty & \text{for } |\mathbf{R}_i - \mathbf{r}_j| < \sigma_{cp}, \\ 0 & \text{otherwise,} \end{cases}$$

where $\beta = (k_B T)^{-1}$ with k_B the Boltzmann constant and where $R_{ij} = |\mathbf{R}_i - \mathbf{R}_j|$. The diameter of the colloids is σ_c , and the distance of closest approach of a colloid and a polymer is $\sigma_{cp} = (\sigma_c + \sigma_p)/2$, with σ_p twice the polymer radius of gyration R_g . We also consider external potentials $u_c(\mathbf{R})$ and $u_p(\mathbf{r})$ acting on the colloids and polymers, respectively, such that the total interaction Hamiltonian of the system of interest here reads $H = H_{cc} + H_{cp} + H_{pp} + U_c + U_p$, where

$$U_c = \sum_{i=1}^{N_c} u_c(\mathbf{R}_i), \quad U_p = \sum_{j=1}^{N_p} u_p(\mathbf{r}_j).$$

The kinetic energy of the polymers and colloids is not considered explicitly here, as it is trivially accounted for in the classical partition sums to be evaluated below.

In this paper, we map the binary mixture of colloids and polymers with interaction Hamiltonian H onto an effective one-component system with Hamiltonian H^{eff} by integrating out the degrees of freedom of the polymer coils. Our deriva-

tion follows closely those of Refs. [12,20,25,26].

It is convenient to consider the system in the (N_c, V, z_p, T) ensemble, in which the fugacity $z_p = \Lambda_p^{-3} \exp(\beta\mu_p)$ of the polymer coils is fixed, with Λ_p the thermal wavelength of species $\nu=c, p$ and with μ_p the chemical potential of the polymers. The thermodynamic potential $F(N_c, V, z_p, T)$ of this ensemble can be written as

$$\exp[-\beta F] = \sum_{N_p=0}^{\infty} \frac{z_p^{N_p}}{N_c! \Lambda_c^{3N_c} N_p!} \text{Tr}_c \text{Tr}_p \exp[-\beta H]$$

$$= \frac{1}{N_c! \Lambda_c^{3N_c}} \text{Tr}_c \exp[-\beta H^{\text{eff}}], \quad (1)$$

where the trace Tr_c is short for the volume integral $\int_V d\mathbf{R}^{N_c}$ over the coordinates of the colloids and similarly for Tr_p . The effective Hamiltonian of the colloids is written as

$$H^{\text{eff}} = H_{cc} + U_c - z_p V_f, \quad (2)$$

where $z_p V_f = z_p V_f(\{\mathbf{R}\})$ is the negative of the grand potential of the fluid of ideal polymer coils in the external potential U_p and in the static configuration of N_c colloids with coordinates $\{\mathbf{R}\}$. Here $V_f(\{\mathbf{R}\})$ is the free volume of the polymers in the configuration of the colloids, weighted by the Boltzmann factor $\exp[-\beta u_p(\mathbf{r})]$ of the external potential. Because of the ideal character of the polymer-polymer interactions, it can be written explicitly as

$$V_f = \int_V d\mathbf{r} \exp \left[-\beta u_p(\mathbf{r}) - \sum_{i=1}^{N_c} \beta \phi_{cp}(|\mathbf{R}_i - \mathbf{r}|) \right]. \quad (3)$$

Nonvanishing contributions to V_f stem from those positions \mathbf{r} that are outside any of the N_c depletion shells. The shape of the free volume is, in general, highly irregular and nonconnected. We decompose V_f , formally, into zero-colloid, one-colloid, two-colloid, etc., contributions by expanding it in terms of the colloid-polymer Mayer function $f(r)$, which for the present model equals -1 for $0 < r < \sigma_{cp}$ and 0 otherwise. One finds

$$V_f = \int_V d\mathbf{r} \exp[-\beta u_p(\mathbf{r})] \prod_{i=1}^{N_c} [1 + f(|\mathbf{R}_i - \mathbf{r}|)]$$

$$= V_f^{(0)} + \sum_{i=1}^{N_c} V_f^{(1)}(\mathbf{R}_i) + \sum_{i < j}^{N_c} V_f^{(2)}(\mathbf{R}_i, \mathbf{R}_j) + \dots, \quad (4)$$

with the zero-colloid term

$$V_f^{(0)} = \int_V d\mathbf{r} \exp[-\beta u_p(\mathbf{r})] \quad (5)$$

and, for $k \geq 1$, the k -colloid contribution

$$V_f^{(k)} = \int_V d\mathbf{r} \exp[-\beta u_p(\mathbf{r})] \prod_{m=1}^k f(|\mathbf{R}_{i_m} - \mathbf{r}|), \quad (6)$$

where only those positions \mathbf{r} give nonvanishing contributions where the depletion layers of (at least) k colloids overlap simultaneously.

We give explicit expressions for $V_f^{(k)}$ for $k=0, 1$, and 2 , in a translationally invariant bulk system, where $U_p \equiv 0$. The zero-body contribution $V_f^{(0)}$ is equal to the total volume of the system V . It follows directly from Eq. (4) that the one-body contribution $V_f^{(1)} = -v_1$ with $v_1 = \pi\sigma_{cp}^3/6$, which can be interpreted as the volume that is excluded for a polymer coil by a single colloid. $V_f^{(2)}(\mathbf{R}_i, \mathbf{R}_j)$ is the lens-shaped overlap volume

$$\beta\phi_{\text{AO}}(R_{ij}) = \begin{cases} -\frac{\pi\sigma_p^3 z_p (1+q)^3}{6 q^3} \times \left[1 - \frac{3R_{ij}}{2(1+q)\sigma_c} + \frac{R_{ij}^3}{2(1+q)^3\sigma_c^3} \right] & \text{for } \sigma_c < R_{ij} < 2\sigma_{cp}, \\ 0 & \text{for } R_{ij} > 2\sigma_{cp}. \end{cases}$$

This Asakura-Oosawa pair potential describes an attractive well close to the surface of the colloid, whose depth increases linearly with increasing z_p . The range of the potential is given by σ_p .

The higher-order contributions $V_f^{(k)}$ correspond to k -body potentials, which will be nonzero when the size ratio $q \geq 0.1547$. In Sec. IV B, we show explicitly that an increasing number of higher-body terms becomes nonzero when q increases. This can be made plausible by geometric arguments, since the number of nonoverlapping colloidal spheres that can simultaneously overlap with a polymer coil increases when q increases. Thus, for large size ratios, three- and more-body interactions cannot be neglected, as also pointed out in Ref. [7]. These authors performed simulations for the AO model, in which the polymers are represented by ideal particles on a cubic lattice [7]. In the work presented here, we investigate the influence of three- and higher-body interactions on the bulk and interfacial phase behavior and structure of the AO model, in which the polymer particles are not restricted to lattice sites. To this end, we developed a simulation method for the AO model, based on the exact effective colloid Hamiltonian, containing all many-body interaction terms. This method was briefly described in Ref. [22] and will be explained in more detail here.

III. SIMULATION METHOD

Calculating the effective Hamiltonian of the colloids in the AO model involves the evaluation of V_f given in Eq. (3), which is computationally extremely demanding by, e.g., a finite-element method because of the highly irregular shape of the volume that contributes to V_f . Here we discuss a method with which *changes* of V_f can be calculated accurately and efficiently, which is then used in a Monte Carlo scheme that generates colloid configurations $\{\mathbf{R}\}$ with the correct Boltzmann weight $\exp[-\beta H^{\text{eff}}]$ to sample phase space in order to evaluate thermal averages of the AO model. This method includes all effective many-body interactions.

The starting point is the expansion of V_f into k -body terms as given in Eq. (4). We separate the $V_f^{(k)}$ terms with k

of two spheres of radius σ_{cp} at separation R_{ij} . Note that these $k=0, 1$ terms are irrelevant offsets that do not affect the thermodynamics and structure of the bulk suspension [20] and that $-z_p\beta^{-1}V_f^{(2)}(R_{ij}) \equiv \phi_{\text{AO}}(R_{ij})$ is the well-known depletion potential of the AO model [1,10]. The exact expression for the potential was derived by Asakura and Oosawa [9] and reads

$=0, 1, 2$, for which analytic expressions exist for some U_p , from those with $k \geq 3$, such that

$$V_f = V_f^{(0)} + \sum_{i=1}^{N_c} V_f^{(1)}(\mathbf{R}_i) + \sum_{i < j}^{N_c} V_f^{(2)}(\mathbf{R}_i, \mathbf{R}_j) + V_f^{(3+)}, \quad (7)$$

where the last term is the accumulation of all $k \geq 3$ contributions given by

$$V_f^{(3+)} = \sum_{k \geq 3} \left[\sum_{i_1 < \dots < i_k}^{N_c} V_f^{(k)}(\mathbf{R}_{i_1}, \dots, \mathbf{R}_{i_k}) \right]. \quad (8)$$

The pairwise additivity approximation is recovered when $V_f^{(3+)}$ is set to zero. Here we go beyond this approximation by a numerical evaluation of $V_f^{(3+)}$; the $k \leq 2$ terms are treated analytically. For the present model an efficient scheme can be constructed by introducing $n = n(\mathbf{r}) \equiv -\sum_{i=1}^{N_c} f(|\mathbf{r} - \mathbf{R}_i|)$, the number of simultaneously overlapping depletion layers in \mathbf{r} . Figure 1 shows a schematic configuration of colloidal particles (solid spheres) and their depletion zones (outer circles)—i.e., the volume that each colloid excludes for the center of mass of a polymer coil. We also plot the values of n for the different regions. It is easy to show that the free volume is given by the integral of $\exp[-\beta u_p(\mathbf{r})]$ over the volume V for which $n=0$, which we write as

$$V_f = \int_{n=0} d\mathbf{r} \exp[-\beta u_p(\mathbf{r})]. \quad (9)$$

As analytic expressions exist for the zero-, one-, and two-body contributions for some U_p , we separate these from V_f . These terms are given by

$$V_f^{(0)} = \int d\mathbf{r} \exp[-\beta u_p(\mathbf{r})],$$

$$\sum_{i=1}^{N_c} V_f^{(1)}(\mathbf{R}_i) = - \int_{n \geq 1} d\mathbf{r} \exp[-\beta u_p(\mathbf{r})] n(\mathbf{r}),$$

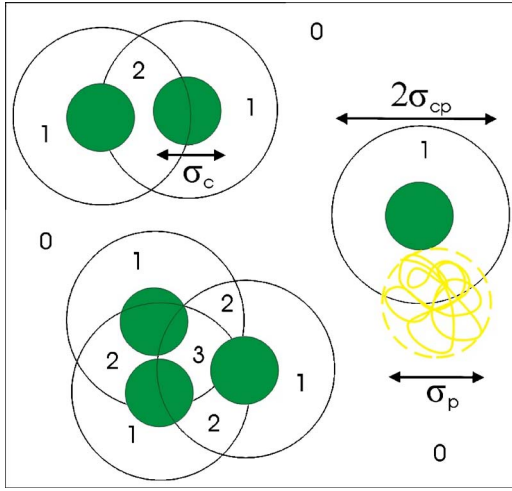


FIG. 1. (Color online) A schematic configuration of colloids (solid circles) with their depletion zones—i.e., the volume that each colloid excludes for the center of mass of a polymer coil. We also plot the values of $n=n(\mathbf{r}) \equiv -\sum_{i=1}^{N_c} f(|\mathbf{r}-\mathbf{R}_i|)$ —i.e., the number of simultaneously overlapping depletion layers—for the different regions. When two colloids approach each other and the depletion zones overlap, there is an increase in the available or free volume for the polymer coils, resulting in an effective attractive interaction between the colloids due to the so-called depletion effect.

$$\begin{aligned} \sum_{i<j}^{N_c} V_f^{(2)}(\mathbf{R}_i, \mathbf{R}_j) &= \int_{n \geq 2} d\mathbf{r} \exp[-\beta u_p(\mathbf{r})] \frac{n(\mathbf{r})!}{(n(\mathbf{r})-2)!2!} \\ &= \int_{n \geq 2} d\mathbf{r} \exp[-\beta u_p(\mathbf{r})] \frac{n(\mathbf{r})(n(\mathbf{r})-1)}{2}. \end{aligned} \quad (10)$$

Combining Eqs. (10) with Eq. (9), V_f can be written as

$$\begin{aligned} V_f &= V_f^{(0)} - \int_{n \geq 1} d\mathbf{r} \exp[-\beta u_p(\mathbf{r})] \\ &= V_f^{(0)} - \int_{n \geq 1} d\mathbf{r} \exp[-\beta u_p(\mathbf{r})] \{n(\mathbf{r}) + [1 - n(\mathbf{r})]\} \\ &= V_f^{(0)} + \sum_{i=1}^{N_c} V_f^{(1)}(\mathbf{R}_i) - \int_{n \geq 2} d\mathbf{r} \exp[-\beta u_p(\mathbf{r})] [1 - n(\mathbf{r})] \\ &= V_f^{(0)} + \sum_{i=1}^{N_c} V_f^{(1)}(\mathbf{R}_i) + \sum_{i<j}^{N_c} V_f^{(2)}(\mathbf{R}_i, \mathbf{R}_j) + V_f^{(3+)}, \end{aligned} \quad (11)$$

with

$$V_f^{(3+)} = -\frac{1}{2} \int_{n \geq 3} d\mathbf{r} \exp[-\beta u_p(\mathbf{r})] [n(\mathbf{r})-1][n(\mathbf{r})-2], \quad (12)$$

where the integration is only over those regions where $n(\mathbf{r}) \geq 3$. This result also follows from inserting the identity

$$\begin{aligned} \sum_{i_1 < \dots < i_k}^{N_c} V_f^{(k)}(\mathbf{R}_{i_1}, \dots, \mathbf{R}_{i_k}) \\ = (-1)^k \int_{n \geq k} d\mathbf{r} \exp[-\beta u_p(\mathbf{r})] \frac{n(\mathbf{r})!}{(n(\mathbf{r})-k)!k!} \end{aligned} \quad (13)$$

into Eq. (8), after a little algebra. Note that Eq. (12) holds strictly for the present Mayer function, whereas Eqs. (7) and (8) hold for any f provided the polymer-polymer interaction is ideal.

Since the standard Metropolis algorithm for Monte Carlo (MC) simulations is based on an acceptance probability $\min(1, \exp[-\beta \Delta H^{\text{eff}}])$, with ΔH^{eff} the change of H^{eff} due to a proposed configuration change, it follows that MC simulations of the AO model can be performed provided the corresponding change $\Delta V_f^{(3+)}$ can be evaluated efficiently—the changes in the two- and one-body terms are easily calculated as in pairwise systems. For MC moves involving only a single colloid—say, $\mathbf{R}_1 \rightarrow \mathbf{R}'_1$ —the only contributions to $\Delta V_f^{(3+)}$ occur inside the two spheres of radius σ_{cp} centered about \mathbf{R}_1 and \mathbf{R}'_1 . In both spheres a spherically symmetric grid with typically $M \approx 2.5 \times 10^5$ grid points \mathbf{r}_m with $1 \leq m \leq M$ is constructed, and from $n(\mathbf{r}_m)$ one can estimate $\Delta V_f^{(3+)}$ using Eq. (12) [22]. We considered the present value of M the optimal balance between accuracy and computational speed.

If $V^{(k)}$ cannot be determined analytically for $k=2,1$ because of a nontrivial $u_p(\mathbf{r})$, one can derive expressions similar to Eq. (12) for $V_f^{(2+)}$ or $V_f^{(1+)}$. In summary, we arrive at H^{eff} given by Eq. (2) with V_f given by Eqs. (11) and (12), and with changes in V_f that can be calculated sufficiently efficiently to be useful in MC simulations, as we will show below.

IV. RESULTS OF SIMULATIONS USING THE EFFECTIVE HAMILTONIAN

A. Bulk phase diagrams

In order to determine the phase diagram of the effective one-component system using our MC scheme, we first calculate the thermodynamic potential F , defined in Eq. (1) with H^{eff} given by Eq. (2), as a function of N_c , V , and z_p . For convenience we usually replace the dependence on z_p by that on the reservoir packing fraction $\eta_p^r \equiv \pi \sigma_p^3 z_p / 6$. As the free energy cannot be measured directly in a Monte Carlo simulation, we use thermodynamic integration to relate the free-energy density $f(\eta_c, \eta_p^r) = \pi \sigma_c^3 F(N_c, V, z_p, T) / 6V$ of the effective system to that of a reference hard-sphere system at the same colloid packing fraction $\eta_c \equiv \pi \sigma_c^3 N_c / 6V$:

$$f(\eta_c, \eta_p^r) = f(\eta_c, \eta_p^r = 0) + f_{\text{attr}}(\eta_c, \eta_p^r), \quad (14)$$

with

$$f_{\text{attr}}(\eta_c, \eta_p^r) = \int_0^{\eta_p^r} d\eta_p^{r'} \left(\frac{\partial f(\eta_c, \eta_p^{r'})}{\partial \eta_p^{r'}} \right) \quad (15)$$

and with $f(\eta_c, \eta_p^r = 0)$ the free-energy density of the pure reference system of hard spheres, for which we use the

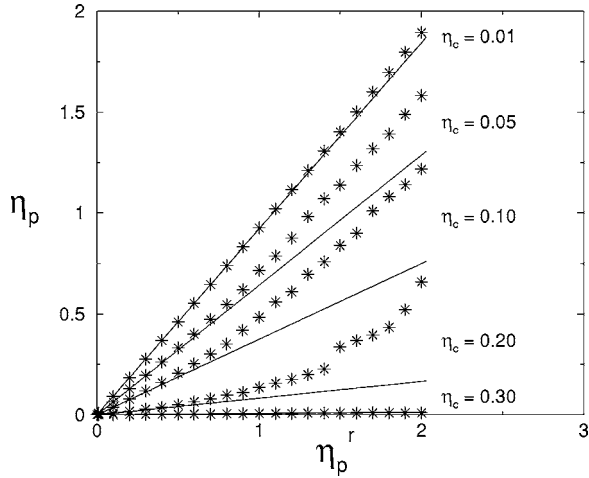


FIG. 2. The polymer packing fraction η_p of a colloid-polymer mixture with size ratio $q=1.0$ versus that of the reservoir η_p^r for several colloid packing fractions η_c . The asterisks denote the simulation data while the solid lines denote the results of the free-volume theory [11,13]. Results like these are used to calculate $\langle \alpha \rangle_{\eta_p^r, \eta_c}$ as defined below Eq. (16).

Carnahan-Starling expressions [27] for the fluid and the analytic form for the equation of state proposed by Hall [28] for the solid phase. In the latter case an integration constant is determined such that the simulation results for fluid-solid coexistence of the pure hard-sphere system are recovered [29]. The integrand in Eq. (15) can be rewritten using Eq. (1) as

$$\left(\frac{\partial \beta f(\eta_c, \eta_p^r)}{\partial \eta_p^r} \right) = - \frac{\langle \alpha \rangle_{\eta_p^r, \eta_c}}{q^3}, \quad (16)$$

where we have introduced the quantity $\langle \alpha \rangle_{\eta_p^r, \eta_c} \equiv \langle \eta_p \rangle / \eta_p^r$ —i.e., the ratio of the density of polymer in the mixture to that in the reservoir—for given polymer reservoir packing fraction η_p^r and colloid packing fraction η_c . The brackets $\langle \dots \rangle$ denote the thermal average over all configurations, weighted by $\exp[-\beta H^{\text{eff}}(\eta_p^r)]$.

In order to map out the phase diagram the free-energy density (14) must be determined from η_p^r integrations for many state points (η_c, η_p^r) . We chose therefore to simulate relatively small systems, with $N_c=128$. We use an equidistant $(r^3, \cos \theta, \phi)$ grid of 100, 50, and 50 points, respectively, to evaluate $V_f^{(3+)}$. In Fig. 2, we plot η_p as a function of η_p^r as measured in a simulation for several η_c and size ratio $q=1$. We also plot η_p as predicted by the free-volume approach [11,13], which is based on the assumption

$$\langle \alpha \rangle_{\eta_p^r} \approx \langle \alpha \rangle_{\eta_p^r=0} \quad (17)$$

and employs scaled particle expressions for the volume that is available for the polymer in a system of pure hard spheres ($\eta_p^r=0$). Figure 2 shows good agreement between the simulation results and those obtained from the free-volume theory for $\eta_c \leq 0.01$ and $\eta_c \geq 0.30$ and for $0.01 < \eta_c < 0.30$ provided $\eta_p^r < 0.8$ (we will show below that the state points for $\eta_p^r > 0.8$ for which we do find deviations with free-volume

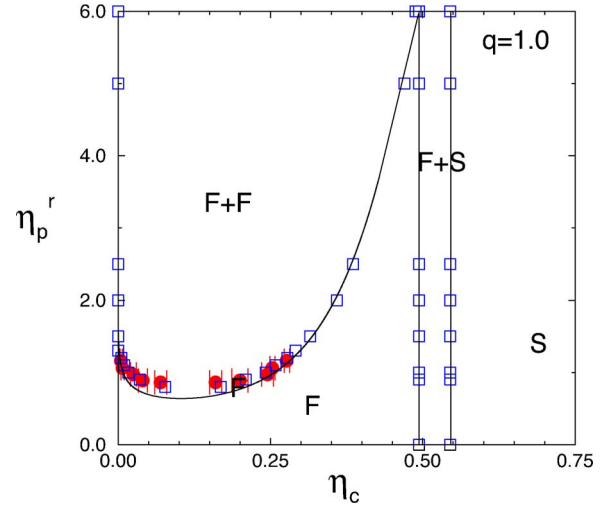


FIG. 3. (Color online) Bulk phase diagram of the AO model (size ratio $q=1$) as a function of the colloid packing fraction η_c and the polymer reservoir packing fraction η_p^r as obtained from simulations of the exact effective one-component Hamiltonian (open squares) and from Gibbs ensemble Monte Carlo simulations using the true binary mixture (solid circles). F and S denote the stable fluid and solid (fcc) phases. $F+S$ and $F+F$ denote, respectively, the stable fluid-solid and fluid-fluid coexistence regions. The solid lines denote the bulk binodals of the free-volume theory [11,13]. Note that all the tielines are horizontal (not drawn).

theory are inside the gas-liquid coexistence region). Using the simulation data for η_p as a function of η_p^r , we calculate the free-energy density $f(\eta_c, \eta_p^r)$ from Eq. (14) by numerical integration. Once f is known, we employ common tangent constructions at fixed η_p^r to obtain the coexisting phases; i.e., we fitted polynomials to f and computed the pressure and chemical potential at each η_c . The densities of the coexisting phases can then be determined by equating the pressures and chemical potentials in both phases. For more details we refer the reader to Ref. [20].

The above procedure has been carried out to determine the phase diagram for size ratio $q=1$. In Fig. 3, we show the resulting phase diagram in the (η_c, η_p^r) plane. The coexisting densities are denoted by the open squares. This representation, which is the natural one given our approach, implies that the tielines connecting coexisting state points are horizontal. At $\eta_p^r=0$ our procedure ensures that we recover the known freezing transition of the pure hard-sphere system. At sufficiently large polymer reservoir packing fraction, we find a liquid-vapor transition with a critical point at $\eta_p^{r,c} \approx 0.86$ and a triple point at $\eta_p^{r,t} \approx 6.0$ at which the colloidal gas, liquid, and solid coexist. Note that the ratio $\eta_p^{r,t} / \eta_p^{r,c} \approx 7$ is remarkably high compared to the corresponding (inverse) temperature ratio in simple fluids. Comparing the present “exact” phase diagram for $q=1$ with the one based solely on pairwise AO interactions, for which the triple and critical point values of η_p^r are ~ 0.8 and ~ 0.5 , respectively [12], shows that the main effect of the many-body interactions is to enhance the η_p^r regime of stable gas-liquid coexistence considerably at the expense of that of the gas-solid coexistence.

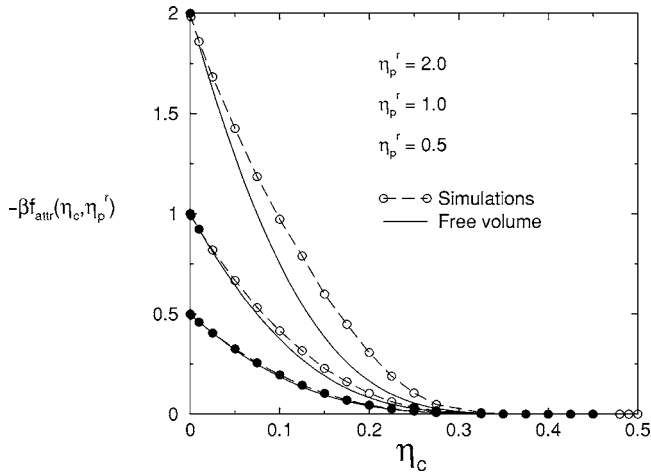


FIG. 4. The free-energy density difference between the AO model (size ratio $q=1.0$) and a pure hard-sphere system $\beta f_{\text{attr}}(\eta_c, \eta_p^r)$ as a function of the colloid packing fraction η_c and for polymer reservoir packing fractions $\eta_p^r=0.5, 1.0$, and 2.0 (from bottom to top). The circles denote the simulation results, while the solid lines denote the predictions from free-volume theory using Eq. (17) [11,13]. Note that excellent agreement is found for all state points in the stable fluid phase (denoted by the solid circles, while the open circles denote the state points in the two-phase region).

In addition, we perform Gibbs ensemble simulations of the true binary mixture; i.e., the polymer coils (modeled as penetrable spheres) are included explicitly in the simulations. In this method, the two coexisting phases are simulated using standard displacement moves in separate simulation boxes which may exchange volume and particles in order to fulfill the phase equilibrium requirements of equal pressures and chemical potentials. The simulation results using the binary mixture agree well with those obtained from an effective one-component system. This is not surprising as the mapping of the binary mixture onto the effective one-component system is exact and no approximations are made to the corresponding effective one-component Hamiltonian. The good agreement also shows that our numerical calculation of the higher-body terms is sufficiently accurate. Note that the Gibbs ensemble simulations of the true binary mixture are only possible fairly close to the critical point.

The solid lines are the results from free-volume theory [11,13]. We find good agreement between both results close to the triple point. The critical point using the free-volume theory is shifted to lower η_p^r with respect to the simulations. In order to appreciate the agreement between the two phase diagrams more, we plot $\beta f_{\text{attr}}(\eta_c, \eta_p^r)$ versus the colloid packing fraction for polymer reservoir packing fractions $\eta_p^r=0.5, 1.0$, and 2.0 . The open circles denote the simulation results for state points in the gas-liquid coexistence region, while the solid circles denote the simulation results for the state points in the stable fluid phase. Figure 4 shows that the free-volume theory—i.e., Eq. (17) with Eqs. (16) and (15)—underestimates βf_{attr} systematically at colloid packing fractions $0.01 < \eta_c < 0.3$ and the deviations become larger at increasing polymer reservoir packing fraction. However, at large polymer reservoir packing fractions, the phase boundaries are located at very small and large colloid packing

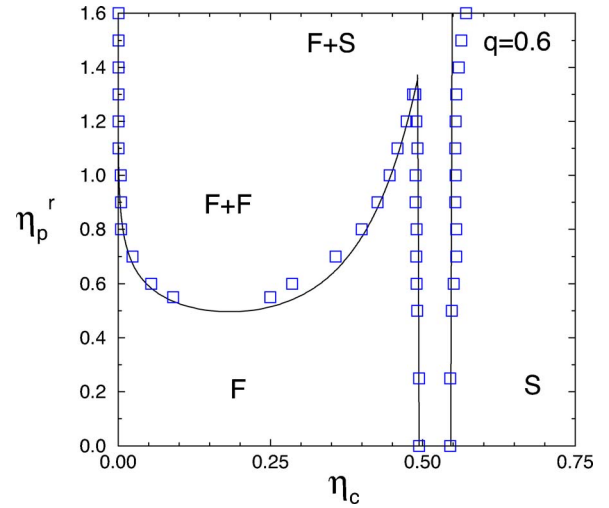


FIG. 5. (Color online) Bulk phase diagram of the AO model (size ratio $q=0.6$) as a function of the colloid packing fraction η_c and the polymer reservoir packing fraction η_p^r as obtained from simulations of the exact effective one-component Hamiltonian (open squares). F and S denote the stable fluid and solid (fcc) phases. $F+S$ and $F+F$ denote, respectively, the stable fluid-solid and fluid-fluid coexistence regions. The solid lines denote the bulk binodals of the free-volume theory [11,13]. Note that all the tielines are horizontal (not drawn).

fractions—i.e., at $\eta_c < 0.01$ and $\eta_c > 0.3$ —where the deviations for βf_{attr} are small. At low polymer reservoir packing fractions, the free-volume theory underestimates βf_{attr} only slightly, resulting in a critical point shifted to lower η_p^r with respect to the simulations. In conclusion, there is excellent agreement between the simulation and free-volume results of βf_{attr} for all state points in the stable fluid phase, yielding good agreement of the two phase diagrams.

Using the same procedure as described above, we also determined the phase diagram for size ratio $q=0.6$. In Fig. 5, we show the resulting phase diagram in the (η_c, η_p^r) plane. Again, we find good agreement with the phase diagram obtained from free-volume theory. At sufficiently large polymer reservoir packing fractions, we find a critical point at $\eta_p^{r,c} \approx 0.53$ and a triple point at $\eta_p^{r,t} \approx 1.35$. The ratio $\eta_p^{r,t} / \eta_p^{r,c} \approx 2.55$ is more than twice as large than the ratio based solely on pairwise AO interactions, for which the triple- and critical-point values of η_p^r are ~ 0.6 and ~ 0.5 , respectively [12]. The enhancement of the bulk liquid regime due to many-body interactions is less pronounced as in the case for $q=1$.

For comparison, we also plot the phase diagram for size ratio $q=0.1$. In this case, the mapping onto the two-body approximation of the effective Hamiltonian is exact, as the three- and higher-body terms are identically zero. The full phase diagram using the Asakura-Oosawa pair potential approximation to the effective Hamiltonian was also determined in Ref. [12] by computer simulations. In Fig. 6, we show the resulting phase diagram in the (η_c, η_p^r) plane along with the one obtained from free-volume theory. We find that the fluid-solid binodal from free-volume theory is shifted to higher η_p^r compared with simulations, while the free-volume

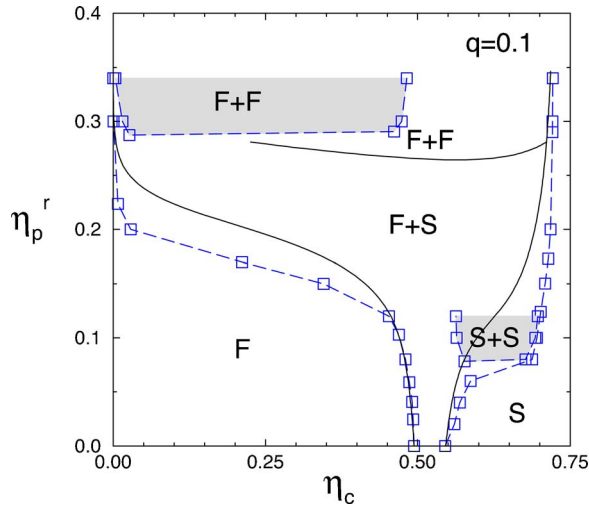


FIG. 6. (Color online) Bulk phase diagram of the AO model (size ratio $q=0.1$) as a function of the colloid packing fraction η_c and the polymer reservoir packing fraction η_p^r as obtained from simulations of the exact effective one-component Hamiltonian (open squares). F and S denote the stable fluid and solid (fcc) phases. $F+S$ denotes the stable fluid-solid coexistence region. The solid lines denote the bulk binodals of the free-volume theory [11,13]. Note that all the tielines are horizontal (not drawn).

theory fluid-fluid binodal is shifted to unphysically high colloid packing fractions.

B. Importance of effective many-body interactions

In Sec. II, we mentioned that an increasing number of higher-body contributions become nonzero upon increasing q . This can easily be understood since the thickness of the depletion layers increases upon increasing q and, hence, the number of depletion layers that can simultaneously overlap increases, upon increasing q . In order to quantify the importance of many-body interactions, we introduce $P(n)$, the probability that we find $n=n(\mathbf{r})$ overlapping depletion layers at \mathbf{r} in a system consisting of N colloids in a volume V and a polymer reservoir packing fraction η_p^r and size ratio q . Using our numerical evaluation of higher-body terms, we can easily measure $P(n)$ in our simulations. In Fig. 7 we show $P(n)$ for size ratios $q=0.1, 0.6$, and 1 , respectively, for varying colloid packing fractions η_c . We set η_p^r to zero as we expect the η_p^r dependence to be small on the basis of Fig. 2 and the good agreement between free-volume theory (using $\eta_p^r=0$ as reference state) and our simulations. For $q=0.1$, we indeed find that $P(n)=0$ for $n \geq 3$. Hence, three- and higher-body interactions are identical to zero and the mapping of the binary colloid-polymer mixture onto an effective Hamiltonian with only effective pair interactions for the colloids is exact for $q=0.1$. We also observe that $P(n=1)$ increases upon increasing η_c as expected, and that $P(n=2)$ increases only slightly for increasing η_c .

For $q=0.6$, we find that $P(n)=0$ for $n \geq 7$ and the importance of many-body interactions, in particular the three-body interactions, increases with η_c . Figure 7 also shows that $P(n)=0$ for $n \geq 8$, when $q=1$. Moreover, we find that the

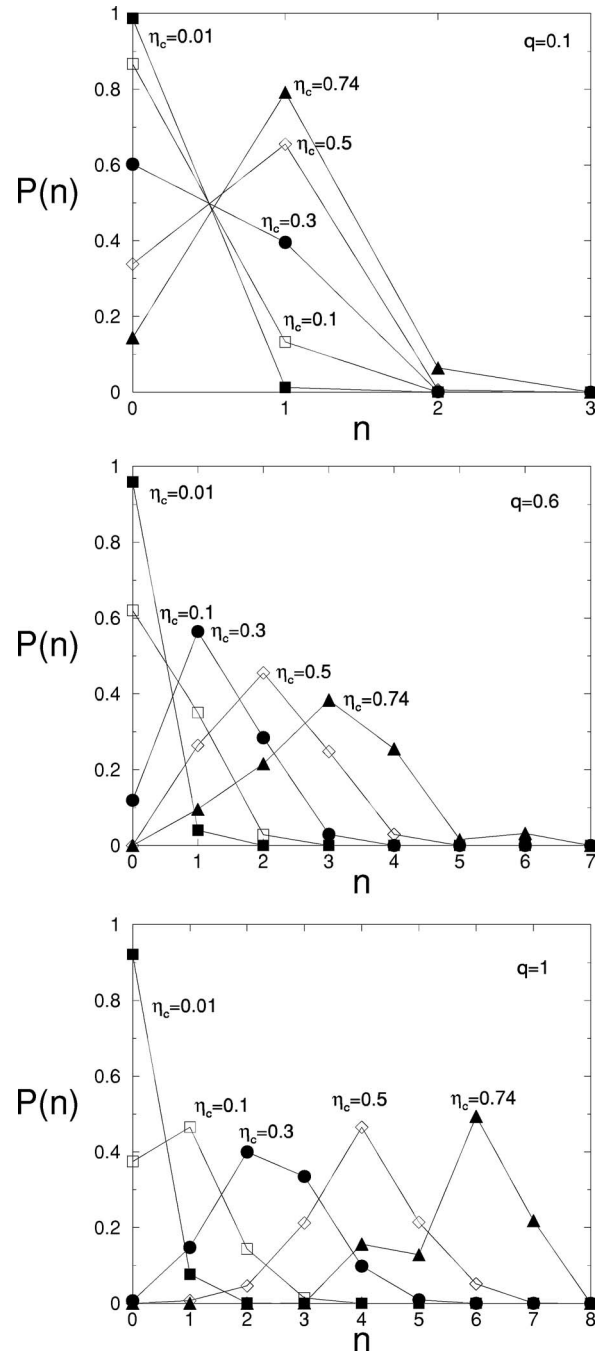


FIG. 7. The probability of n overlapping depletion layers for a colloid-polymer mixture with polymer reservoir packing fraction $\eta_p^r=0$ and colloid packing fraction $\eta_c=0.01$ (■), 0.1 (□), 0.3 (●), 0.5 (◇), and 0.74 (▲) as labeled for varying size ratios $q=0.1, 0.6$, and 1.0 from top to bottom.

dominant contribution to the effective interaction changes from the zero-body term to the six-body term upon increasing η_c .

C. Structure

In this subsection we turn attention to the structure of the model colloid-polymer mixture for $q=1$. Given that we de-

terminated the phase diagrams in Sec. IV A, we can now calculate the colloid-colloid, colloid-polymer, and polymer-polymer radial distribution function $g(r)$ and the structure factor $S(k)$ in the fluid phase but close to the phase boundaries. We performed simulations with $N_c=1000$ colloids, interacting with the full effective Hamiltonian obtained by integrating out the degrees of freedom of the polymer. At first sight it may seem surprising that it is possible to recover information about the structure of the polymer as we traced out the polymer degrees of freedom. However, as the polymer coils are ideal, the number density of the polymer is constant ($\rho_p=\rho_p^f$) in the free volume or the holes of the system. The colloid-polymer and polymer-polymer correlations can therefore be obtained from the colloid-hole and hole-hole correlations. More precisely, we determine the colloid-polymer and polymer-polymer correlations from 10 000 randomly inserted polymer coils in an instantaneous colloid configuration, provided that no overlap exists between the polymer and colloids. This procedure breaks down in practice when the probability to insert a polymer is smaller than about 10^{-4} . Our procedure for calculating the colloid-polymer and polymer-polymer correlations is therefore restricted to colloid packing fractions $\eta_c < 0.4$. The structure factor $S_{\alpha\beta}(k)$ is calculated using $S_{\alpha\beta}(k) = (N_\alpha N_\beta)^{-1/2} \langle \rho_\alpha(\mathbf{k}) \rho_\beta(-\mathbf{k}) \rangle$, where $\rho_\alpha(\mathbf{k}) = \sum_{i=1}^{N_\alpha} \exp(i\mathbf{k} \cdot \mathbf{r}_i)$. In Figs. 8–11 we show $g_{\alpha\beta}(r)$ and $S_{\alpha\beta}(k)$ for four different state points, where $g_{\alpha\beta}(r)$ is the radial distribution function. The packing fractions of the statepoints are given in Table I.

Figure 8 shows the colloidal structure factor $S_{cc}(k)$ and radial distribution function $g_{cc}(r)$ of the effective one-component system using the full effective Hamiltonian in simulations with size ratio $q=1$, polymer reservoir packing fraction $\eta_p^f=4.8$, and colloid packing fraction $\eta_c=0.48$. The colloid packing fraction was too high for our procedure to calculate the colloid-polymer and polymer-polymer correlations as the probability to insert a polymer in a typical colloid configuration is extremely small ($\approx 10^{-7}$). For comparison, we also plot the Percus-Yevick (PY) results for $g_{cc}(r)$ and $S_{cc}(k)$ of a pure system of hard spheres at the same colloid packing fraction. We find good agreement between the PY result and the simulation, showing that the structure of the colloids in the mixture is close to that of pure hard spheres. This result supports the validity of assumption (17) in the free-volume theory at high colloid packing fractions. We also show the three partial radial distribution functions obtained from density functional theory (DFT) of the binary mixture. For our DFT calculations, we employ the test particle approach, in which one particle of the mixture is fixed at the origin and thereby acts as an external potential for the rest of the mixture. For $g_{cc}(r)$ and $g_{cp}(r)$ we fix a colloid, which generates a hard-sphere potential for both the colloids and polymer. By minimizing the density function $\Omega[\rho_c, \rho_p]$ we obtain the density distributions $\rho_{cc}(r)$ and $\rho_{cp}(r)$ of the colloids and polymer, respectively, in the external field exhibited by a colloid. From those density distributions the partial radial distribution functions follow directly by $g_{cc}(r) = \rho_{cc}(r)/\rho_c$ and $g_{cp}(r) = \rho_{cp}(r)/\rho_p$. We use the same strategy in order to obtain $g_{pc}(r)$ and $g_{pp}(r)$ —however, now we have to fix a polymer at the origin, which exhibits an external

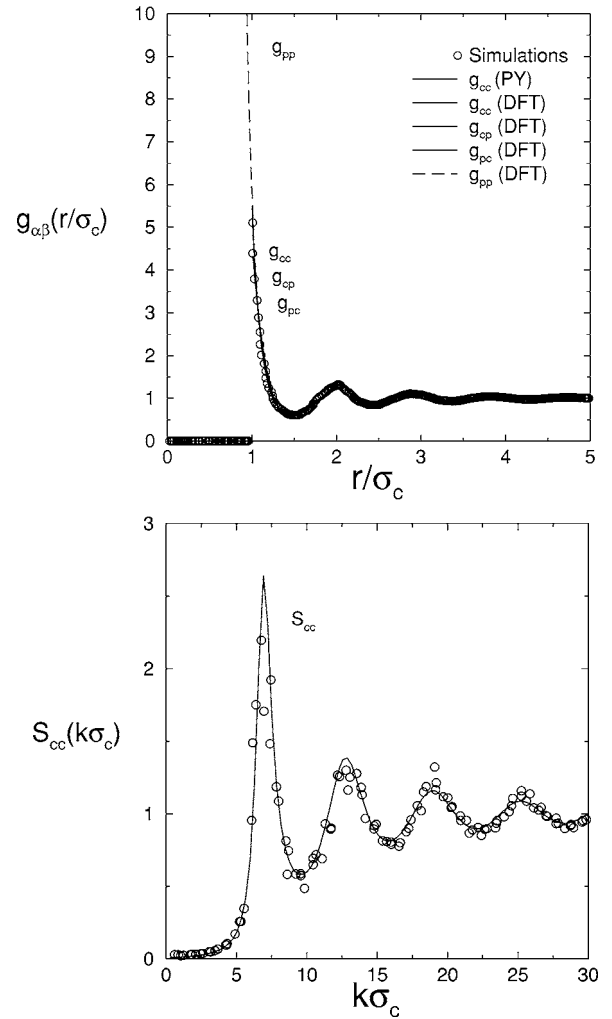


FIG. 8. Colloid-colloid radial distribution function $g_{cc}(r)$ (top) and structure factor $S_{cc}(k)$ (bottom) of the effective one-component system (open circles) using the full effective Hamiltonian in simulations with size ratio $q=1$, polymer reservoir packing fraction $\eta_p^f=4.8$, and colloid packing fraction $\eta_c=0.48$. The solid lines are the PY results for $S_{cc}(k)$ and $g_{cc}(r)$ of a pure system of hard spheres at a packing fraction $\eta_c=0.48$. The DFT results for the colloid-colloid and colloid-polymer radial distribution functions of the binary mixture are also denoted by solid lines, but are indistinguishable from each other and from the PY result. The polymer-polymer radial distribution function $g_{pp}(r)$ obtained from DFT is denoted by the dashed line and DFT yields $g_{pp}(r=0) \approx 7 \times 10^6$.

potential only on the colloid components. The polymer in the mixture feels this external field only indirectly through the inhomogeneous distribution of colloids. Again we obtain density distributions $\rho_{pc}(r)$ and $\rho_{pp}(r)$ from which the partial radial distribution functions $g_{pc}(r) = \rho_{pc}(r)/\rho_c$ and $g_{pp}(r) = \rho_{pp}(r)/\rho_p$ follow. It is interesting to note that through the asymmetry in the external field exhibited by either a colloid or a polymer one finds that $g_{cp}(r) \neq g_{pc}(r)$, despite the fact that the functional we minimized predicts symmetric direct correlation functions—i.e., $c_{cp}^{(2)}(r) = c_{pc}^{(2)}(r)$. We have verified that while the shape of $g_{pp}(r)$ depends on both η_c and η_p^f , in the limit $r \rightarrow 0$ we obtain the correct behavior $g_{pp}(r \rightarrow 0) \rightarrow 1/\alpha$, which depends only on the colloid packing fraction

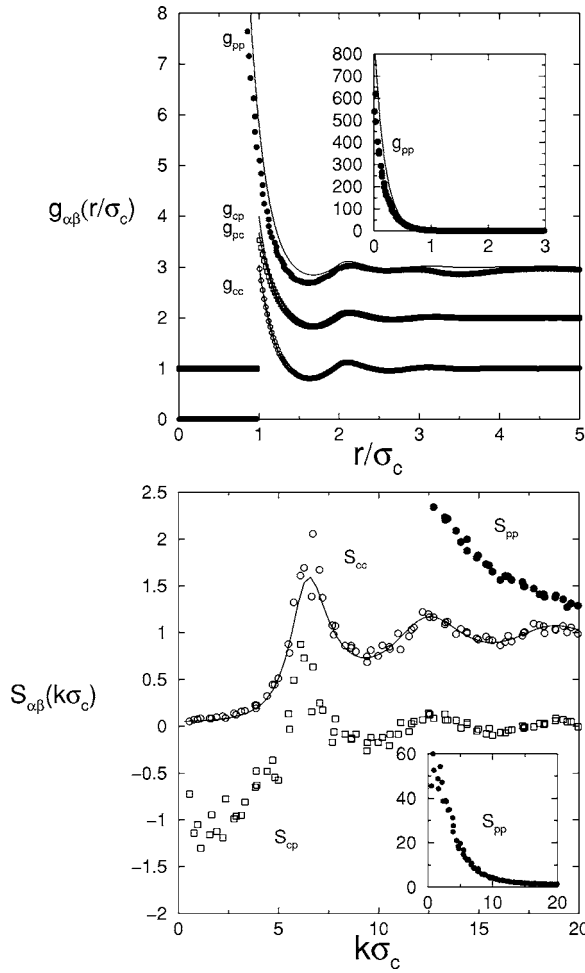


FIG. 9. Colloid-colloid (open circles), colloid-polymer (open squares), and polymer-polymer (solid circles) partial radial distribution functions $g_{\alpha\beta}(r)$ (top) and structure factors $S_{\alpha\beta}(k)$ (bottom) of the effective one-component system using the full effective Hamiltonian in simulations with size ratio $q=1$, polymer reservoir packing fraction $\eta_p^r=1.65$, and colloid packing fraction $\eta_c=0.35$. The solid lines are the PY results for $g_{cc}(r)$ and $S_{cc}(k)$ of pure hard spheres at a packing fraction $\eta_c=0.35$. The DFT results for the three partial radial distribution functions of the binary mixture are also denoted by solid lines. The DFT result for $g_{cc}(r)$ is indistinguishable from the PY result. For clarity, $g_{cp}(r)$ and $g_{pp}(r)$ are shifted in the vertical direction. The insets show $g_{pp}(r)$ and $S_{cc}(k)$ at a larger scale.

η_c . This result can easily be seen if one realizes that the probability to find a second polymer close to the first polymer that found an empty hole in a fixed colloid configuration is $1/\alpha$ times higher than for two polymers infinitely far apart from each other. Figure 8 shows that all partial $g_{\alpha\beta}(r)$'s from DFT are indistinguishable from the PY result and from each other, except that the polymer-polymer radial distribution function continues for $r < \sigma_c$ and rises steeply for $r \rightarrow 0$. Density functional theory yields $g_{pp}(r=0) \simeq 7 \times 10^6$.

Figure 9 shows the colloid-colloid, colloid-polymer, and polymer-polymer radial distribution functions and structure factors from simulations for polymer reservoir packing fraction $\eta_p^r=1.65$ and colloid packing fraction $\eta_c=0.35$. The

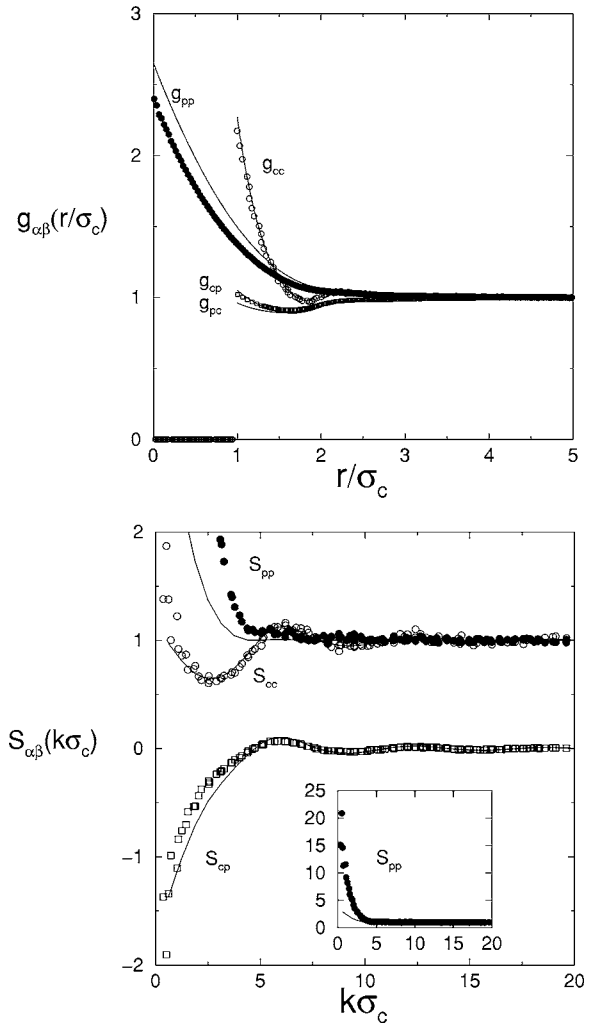


FIG. 10. Colloid-colloid (open circles), colloid-polymer (open squares), and polymer-polymer (solid circles) partial radial distribution functions $g_{\alpha\beta}(r)$ (top) and structure factors $S_{\alpha\beta}(k)$ (bottom) of the effective one-component system using the full effective Hamiltonian in simulations with size ratio $q=1$, polymer reservoir packing fraction $\eta_p^r=0.5$, and colloid packing fraction $\eta_c=0.1$. The solid lines are the PY results for the three partial structure factors $S_{\alpha\beta}(k)$ of the binary mixture (bottom figure) and the DFT results for the three partial radial distribution functions $g_{\alpha\beta}(r)$ of the binary mixture (top figure). The inset shows $S_{pp}(k)$ at a larger scale.

most striking feature is the similarity of the colloid-colloid and colloid-polymer structure factors and radial distribution functions, while again a very large value is found for $g_{pp}(r)$ as $r \rightarrow 0$ and a steep rise for $S_{pp}(k)$ as $k \rightarrow 0$. For comparison, we also show the Percus-Yevick (PY) result for $g_{cc}(r)$ and $S_{cc}(k)$ of pure hard spheres at the same colloid packing fraction. We were not able to find a PY solution for the binary AO model. We find good agreement between the PY result and the simulations, showing again that the structure of the colloids in the mixture is close to that of pure hard spheres. We also show the three partial radial distribution functions obtained from DFT of the binary mixture. We find that $g_{cc}(r)$ is indistinguishable from the PY result, and we find good agreement between the simulations and DFT, although there are small deviations for $g_{pp}(r)$.

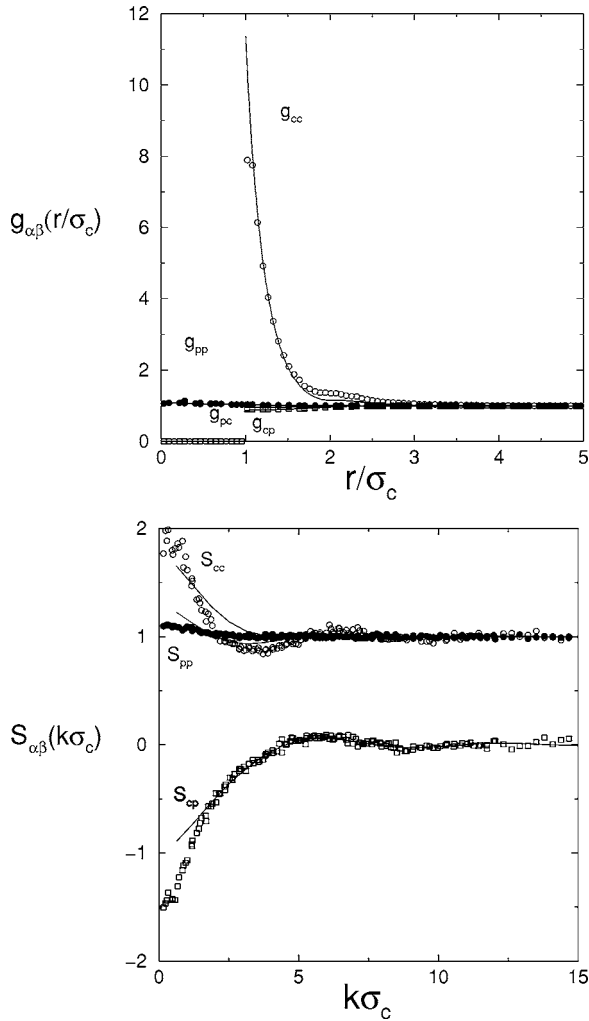


FIG. 11. Colloid-colloid (open circles), colloid-polymer (open squares), and polymer-polymer (solid circles) partial radial distribution functions $g_{\alpha\beta}(r)$ (top) and structure factors $S_{\alpha\beta}(k)$ (bottom) of the effective one-component system using the full effective Hamiltonian in simulations with size ratio $q=1$, polymer reservoir packing fraction $\eta_p^r=1.0$, and colloid packing fraction $\eta_c=0.01$. The solid lines are the PY results for the three partial structure factors $S_{\alpha\beta}(k)$ of the binary mixture (bottom figure) and the DFT results for the three partial radial distribution functions $g_{\alpha\beta}(r)$ of the binary mixture (top figure).

In Fig. 10, we show the simulation results for the partial radial distribution functions $g_{\alpha\beta}(r)$ and structure factors $S_{\alpha\beta}(k)$ for a polymer reservoir packing fraction $\eta_p^r=0.5$ and colloid packing fraction $\eta_c=0.1$, which is close to the critical point. All three partial structure factors $S_{\alpha\beta}(k)$ exhibit a steep rise as $k \rightarrow 0$, characteristic of Ornstein-Zernike behavior. For comparison, we plot the PY results for the three partial structure factors of the binary AO model and we find reasonable agreement for the colloid-colloid and colloid-polymer structure factors. The small-angle polymer-polymer scattering is largely underestimated in the PY result compared with simulations. We also show the three partial radial distribution functions obtained from DFT of the binary mixture. We find good agreement for the colloid-colloid and colloid-polymer radial distribution functions and small deviations for the

TABLE I. The state points at which the partial structure factors and radial distribution functions were determined in terms of the colloid packing fraction η_c and the polymer reservoir packing fraction η_p^r , all for size ratio $q=1$.

State point	η_c	η_p^r
A	0.48	4.8
B	0.35	1.65
C	0.1	0.5
D	0.01	1.0

polymer-polymer radial distribution function.

Figure 11 shows the simulation results for the partial radial distribution functions $g_{\alpha\beta}(r)$ and structure factors $S_{\alpha\beta}(k)$ for a polymer reservoir packing fraction $\eta_p^r=1.0$ and colloid packing fraction $\eta_c=0.01$. For comparison, we also plot the PY results for the three partial structure factors of the binary AO model, which deviate considerably from the simulation results. We also show the three partial radial distribution functions obtained from DFT, and we find good agreement with the simulation results. We note that hardly any structure appears in the polymer-polymer radial distribution function and structure factor as the colloid packing fraction is very low and the polymers are treated as ideal particles.

D. Adsorption at a hard wall

We now consider the AO model with $q=1$ in contact with a planar hard wall at $z=0$ —i.e., such that $\beta u_p(z)=\beta u_c(z)=0$ for $z > \sigma_c/2$ ($=\sigma_p/2$) and ∞ for $z < \sigma_c/2$, with z the distance of a particle from the wall. One then finds from Eq. (6) for $k=1$ that the effective, polymer-induced wall-colloid potential $-z_p\beta^{-1}V_f^{(1)}(z)$ is attractive if $z < \sigma_p + \sigma_c/2$, with a strength similar to that of the bulk colloid-colloid depletion potential $\phi_{AO}(R_{ij})$ [26]. On the basis of the attractive one-body potential one expects preferential colloid adsorption by the hard wall. Moreover, given the large η_p^r interval $[\eta_p^{r,c}, \eta_p^{r,l}]$ with a stable gas-liquid binodal, one might expect, by analogy with simple fluids, a wetting transition at some $\eta_p^r = \eta_p^{r,w}$ in this interval [30]. However, unlike the case of simple fluids the pair interaction $-z_p\beta^{-1}V_f^{(2)}(\mathbf{R}_i, \mathbf{R}_j)$ is now a nontrivial function of \mathbf{R}_i and \mathbf{R}_j for two colloids close to the wall, with a strength that is reduced considerably compared to its translationally invariant bulk form $\phi_{AO}(R_{ij})$ [26]. This reduction, which is caused by an overlap of the pairwise “lens” with the wall, tempers the tendency to form a dense liquid layer at contact and thus competes with the attractive one-body potential. The effect of the k -body interactions with $k \geq 3$ on the adsorption is less clear. Here we investigate the adsorption with a grand canonical version of our MC scheme, which includes all many-body effects. We measured the equilibrium colloid density profile $\eta_c(z)$ at fixed η_p^r in a rectangular box of volume $A \times L$. Here A is the area of the hard wall, along which we apply periodic boundary conditions, and $L=50\sigma_c$ the box length perpendicular to the wall such that $0 < z < L$. We use the technique of Ref. [31] to impose a flat average profile $\eta_c(z)=\eta_c^b$ for $L-2\sigma_c \leq z \leq L$,

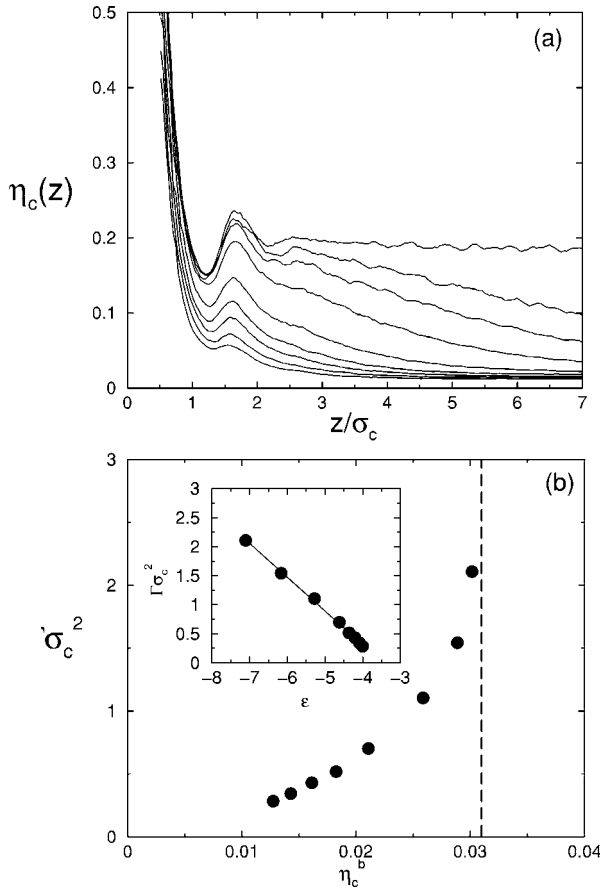


FIG. 12. (a) Colloid density profiles $\eta_c(z)$ for several fugacities (asymptotic colloid bulk densities η_c^b), near a hard wall at $z=0$. The reservoir polymer packing fraction is $\eta_p^f=0.9$, and the size ratio $q = \sigma_p/\sigma_c=1$. (b) The adsorption $\Gamma\sigma_c^2$ upon approach of gas saturation η_c^{sat} (dashed vertical line). The inset shows that the adsorption $\Gamma\sigma_c^2$ appears to diverge as $-\xi\epsilon$ with $\epsilon \equiv \ln(\eta_c^{sat} - \eta_c^b)$ and ξ the bulk correlation length (see text). The solid line denotes a linear fit.

where the bulk packing fraction η_c^b is fixed by the chemical potential. For all state points considered the density profile is found to be constant in $10\sigma_c < z < L$; i.e., we mimic a semi-infinite bulk gas in contact with a hard wall.

In Fig. 12 we show the density profile $\eta_c(z)$ in the vicinity of the hard wall for $\eta_p^f=0.9$ at several $\eta_c^b < \eta_c^{sat}$, the saturated colloid gas density. The exact values of η_c^b can be found in Fig. 12(b), where we show the corresponding dimensionless adsorption $\Gamma\sigma_c^2 = \int_0^L dz (\eta_c(z) - \eta_c^b) / \sigma_c$ as a function of η_c^b . The formation of a thick liquid film and the logarithmic increase of $\Gamma\sigma_c^2$ as $\eta_c^b \rightarrow \eta_c^{sat}$ in Fig. 12(a) are strongly indicative of complete wetting at $\eta_p^f=0.9$. From the slope of the inset in Fig. 12(b) one obtains the correlation length $\xi = (0.58 \pm 0.01)\sigma_c$ of the wetting phase [30], which agrees well with $\xi = (0.60 \pm 0.04)\sigma_c$ as determined from the asymptotic decay of the radial distribution function of the bulk coexisting liquid at the value of η_p^f . Figure 13 shows typical colloid configurations for $\eta_p^f=0.9$ at $\eta_c^b=0.013$ ($\approx 0.42\eta_c^{sat}$) and at $\eta_c^b=0.029$ ($\approx 0.94\eta_c^{sat}$). We clearly observe the formation of a thick liquid film at the wall upon approaching bulk coexistence. Note that the interface between the adsorbed liquid

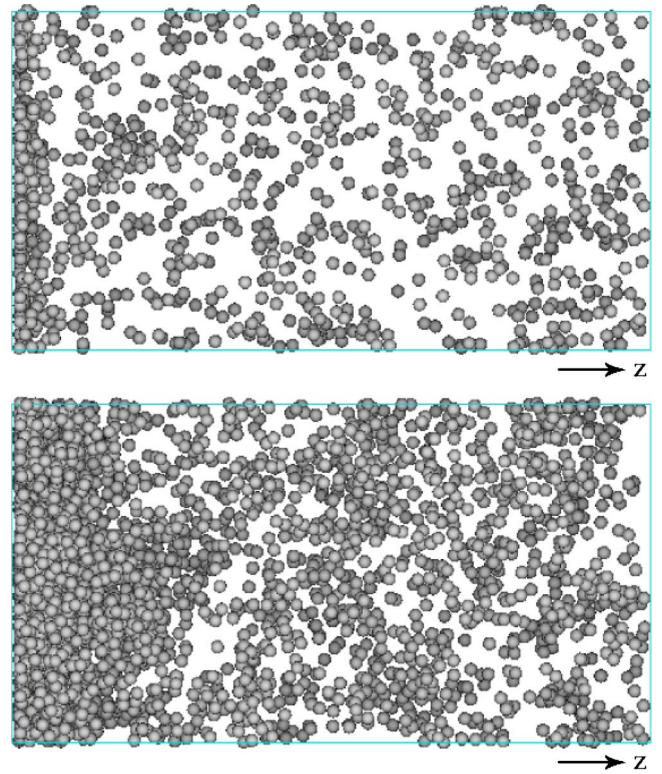


FIG. 13. (Color online) Typical colloid configurations of the adsorption of a colloid-polymer mixture with size ratio $q=1$ at a planar hard wall obtained from Monte Carlo simulations based on the exact effective one-component Hamiltonian for the colloids. The polymer reservoir packing fraction is $\eta_p^f=0.9$, and the colloid packing fraction is $\eta_c^b=0.013$ (top) and 0.029 (bottom).

film and the gas phase shows huge density fluctuations as the interfacial tension is very small [16,17].

For $q=1$ we also studied the density profiles $\eta_c(z)$ and the adsorption Γ for $\eta_p^f=1.0$ and 1.05 . The case $\eta_p^f=1.0$ is shown in Fig. 14 for several $\eta_c^b < \eta_c^{sat}$; the figure for the case $\eta_p^f=1.05$ can be found in Ref. [23]. Again the formation of a thick liquid film and the logarithmic increase of $\Gamma\sigma_c^2$ provide evidence for complete wetting for $\eta_p^f=1.0$ and 1.05 . The correlation length determined from the slope of $\Gamma\sigma_c^2 \propto \epsilon$ upon approach of saturation is $\xi = (0.54 \pm 0.01)\sigma_c$ and $\xi = (0.55 \pm 0.01)\sigma_c$ for $\eta_p^f=1.0$ and 1.05 , respectively, which agree well with $\xi = (0.56 \pm 0.04)\sigma_c$ and $\xi = (0.55 \pm 0.04)\sigma_c$ as determined from the asymptotic decay of the radial distribution function.

Figure 15 shows the density profiles $\eta_c(z)$ for $\eta_p^f=1.12$ at several $\eta_c^b < \eta_c^{sat}$ along with the corresponding dimensionless adsorption in the inset. The finite Γ for $\eta_c^b \rightarrow \eta_c^{sat}$ and the finite liquid film thickness in Fig. 15 imply partial wetting at $\eta_p^f=1.12$. Indeed partial wetting was observed for all $\eta_p^f \geq 1.10$ that we considered. This implies that the wetting transition occurs at $\eta_p^{r,w}$ with $1.05 < \eta_p^{r,w} < 1.10$. Despite considerable effort we did not find any evidence for a *prewetting* transition—i.e., a transition from a thin to a thick liquid film—which by analogy with simple liquids is to be expected in the complete wetting regime $\eta_p^f \leq \eta_p^{r,w}$ if the wetting transition is first order [30].

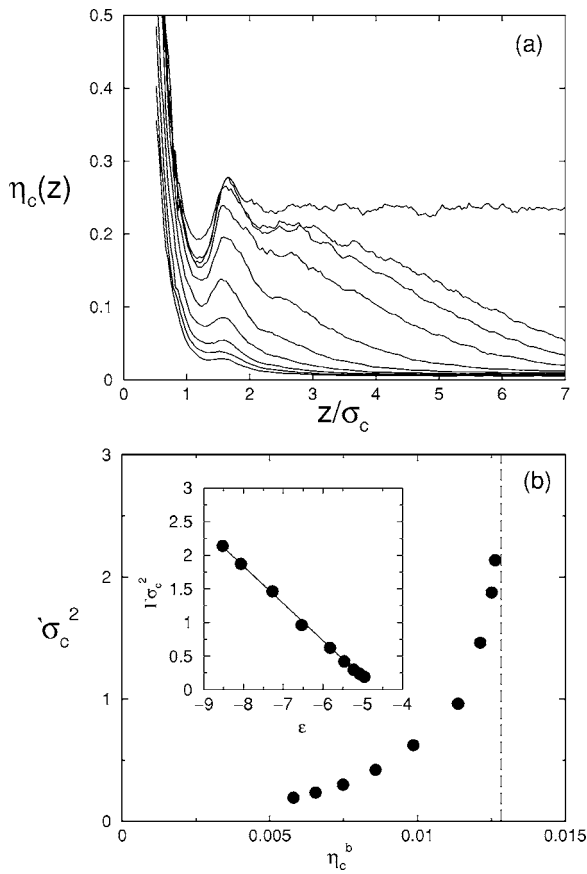


FIG. 14. Same as Fig. 12, but for $\eta_p^r=1.0$.

In accordance with the DFT results of Refs. [25,32], we did find off-coexistence jumps $\delta\Gamma$ in Γ in three separate regimes $\eta_p^r > \eta_p^{r,w}$ —i.e., in the partial wetting regime. The inset of Fig. 15 shows such a jump, which we associate, following Refs. [25,32], with a layering transition (even though the adsorption is not strictly localized in a well-defined layer). From the profiles in Fig. 15 one checks that $\delta\Gamma$ is due to a condensation in a regime $2\sigma_c \leq z \leq 6\sigma_c$. Typical colloid configurations just before and after the jump in the adsorption are shown in Fig. 16. This “third” layering transition was also found at $\eta_p^r=1.10$, although slightly further off coexist-

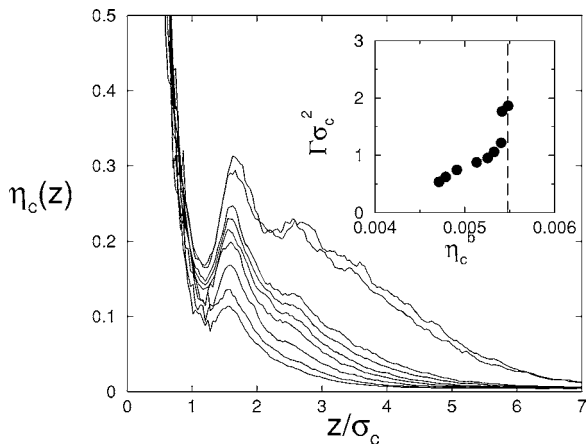


FIG. 15. Same as Fig. 12, but for $\eta_p^r=1.12$.

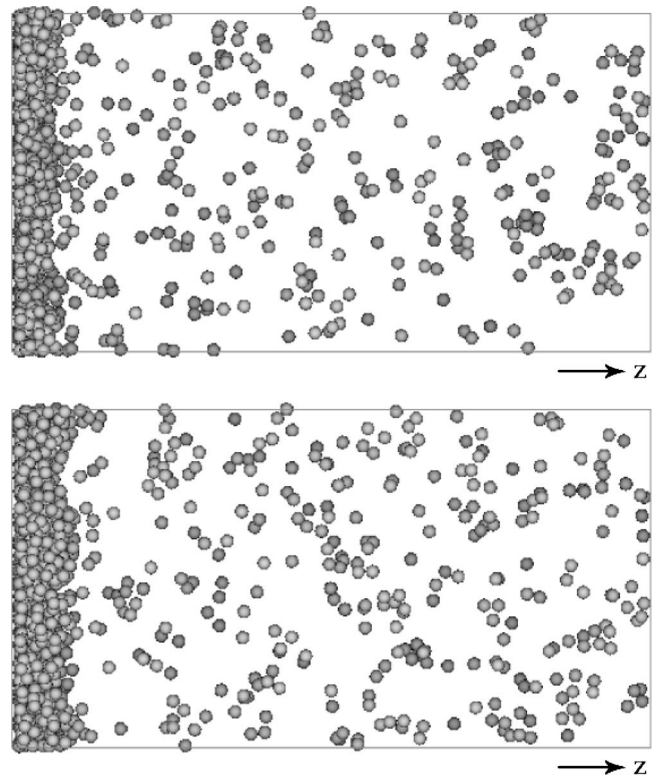


FIG. 16. Typical colloid configurations of the adsorption of a colloid-polymer mixture with size ratio $q=1$ at a planar hard wall obtained from Monte Carlo simulations based on the exact effective one-component Hamiltonian for the colloids. The polymer reservoir packing fraction is $\eta_p^r=1.12$, and the colloid fraction is $\eta_c^b=0.00534$ (top) and 0.00539 (bottom), reflecting the “third” layering transition.

ence and with a smaller $\delta\Gamma$. At yet smaller η_p^r we did not detect any discontinuity in the adsorption, consistent with a low- η_p^r critical point for a line of layering transitions. Figure 17 shows a similar adsorption discontinuity, which can be associated with the second layering transition for $\eta_p^r=1.2$, while Fig. 18 shows one corresponding to the first layering transition for $\eta_p^r=1.24$. The jump in the first is due to adsorption in $0.7\sigma_c \leq z \leq 3\sigma_c$ and that in the second in $1.5\sigma_c \leq z$

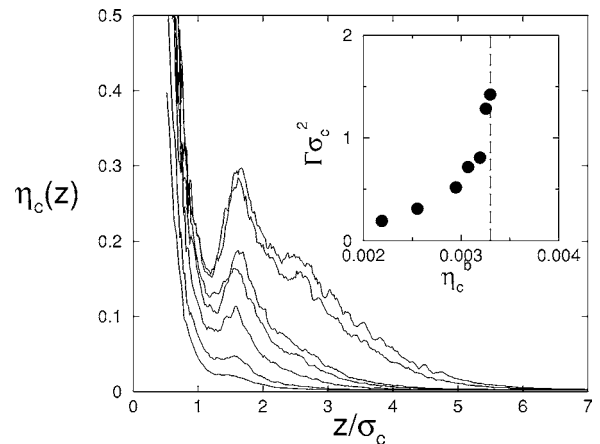


FIG. 17. Same as Fig. 12, but for $\eta_p^r=1.2$.

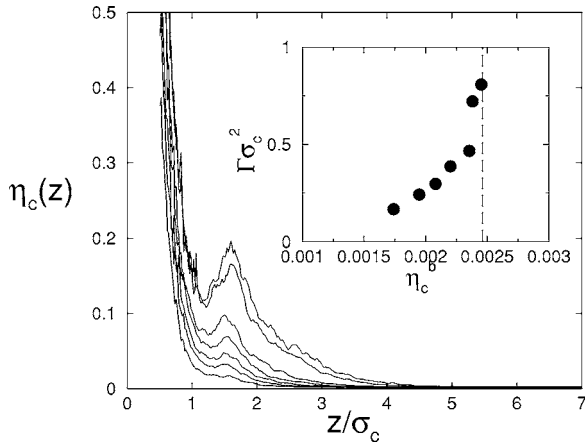


FIG. 18. Same as Fig. 12, but for $\eta_p^r=1.24$.

$\leq 4\sigma_c$. Note that all three layering transitions take place just below saturation, are entropy driven, occur only for $\eta_p^{r,w} < \eta_p^r \leq \eta_p^{r,t}$, extend over a rather small regime of η_p^r , and seem to end in their own (surface) critical point. We stress that our results are in qualitative agreement with density functional predictions for the AO model [25,32].

Finally, we show the surface phase diagram in Fig. 19 as obtained from our adsorption studies for varying η_p^r . Figure 19 shows the layering transitions on an expanded scale, while the inset shows all values of η_p^r that we considered. The solid line denotes that part of the saturated gas branch that is relevant for our wetting and layering study. The full bulk phase diagram for $q=1$ was already shown in Fig. 3. The dashed curve in the inset is the gas binodal as predicted by the “free volume theory” of Refs. [11,13], where the free volume is accounted for within first-order perturbation theory by its average in a pure hard-sphere system. On the

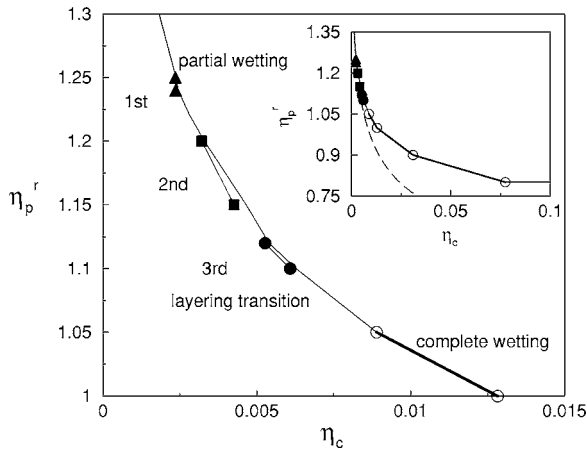


FIG. 19. Surface phase diagram of the AO model (size ratio $q=1$) as a function of the colloid packing fraction η_c and polymer reservoir packing fraction η_p^r . The solid curve denotes the saturated bulk gas branch, separated into a regime of complete wetting [thick curve (○)], and partial wetting by colloidal liquid (thin curve) at a planar hard wall. The first (▲), second (■), and third (●) layering transitions are off bulk coexistence. The inset shows the surface phase diagram on a larger scale. The dashed curve in the inset denotes the bulk binodal of the “free-volume theory” [11,13].

full scale of Fig. 3 this approximation turns out to be remarkably accurate. However, on the detailed scale of the gas branch in the inset, the deviations are appreciable—e.g., a factor of about 2 in η_c at $\eta_p^r=0.9$. The different symbols denote the varying η_p^r that we used in our adsorption studies. The complete wetting regime is denoted by the thick curve and (○), while the partial wetting regime is represented by the thin curve. Figure 19 shows clearly that the first (▲), second (■), and third (●) layering transitions take place off bulk coexistence, but only slightly.

V. CONCLUSIONS

We have studied a model suspension of colloidal hard spheres and nonadsorbing ideal polymer in bulk and adsorbed against a planar hard wall. By first integrating out the degrees of freedom of the polymer coils in the partition function we derive a formal expression for the effective Hamiltonian of the colloids. For sufficiently large polymer coils compared to the colloids, the effective Hamiltonian consists of (trivial) zero- and one-body terms, but also effective polymer-mediated two- and higher-body terms. We developed an efficient Monte Carlo simulation scheme for a model colloid-polymer mixture, based on the exact effective Hamiltonian; i.e., it incorporates all many-body interactions. We show explicit phase diagrams for size ratios $q=\sigma_p/\sigma_c=1, 0.6$, and 0.1 and find good agreement with the predictions obtained from free-volume theory. In addition, we studied the adsorption of the mixture against a planar hard wall. We found a very rich surface phase diagram with a wetting transition from complete wetting to partial wetting and a number of layering transitions. Our results are in good agreement with recent DFT predictions [25,32]. The many-body character of the polymer-mediated effective interactions between the colloids yields a bulk phase behavior and adsorption phenomena that differ substantially from those found for pairwise simple fluids: e.g., we find an anomalously large bulk liquid regime and, far from the bulk triple point, three layering transitions in the partial wetting regime.

However, experiments [3,5,6] show that the bulk liquid regime is much smaller than predicted by our results of the AO model. A recent simulation study showed that quantitative agreement with experiments was found by including excluded-volume interactions between the polymers [8]. More specifically, the bulk liquid regime—i.e., $\eta_p^{r,t}/\eta_p^{r,c}$ —decreases enormously. What the repercussions of the polymer interactions are on the wetting behavior—e.g., the location of the wetting transition and the layering transitions—remains an open question. Recent contact angle measurements show indications that there is a transition from partial to complete wetting for a mixture of silica spheres and PDMS [33]. However, confocal microscopy experiments on silica-PDMS mixtures show a thick colloidal liquid layer adsorbed at the glass wall consistent with complete wetting for all measured state points [34]. These authors were unable to find a wetting transition from complete to partial wetting. The interfacial tension and wetting behavior was recently

calculated using the free-volume approach extended to interacting polymers [35]. Investigations whether or not a wetting transition occurs in a mixture of colloids and *interacting* polymers using the coarse-graining techniques of Ref. [8] are in progress.

Finally, we note that our simulation scheme can easily be extended to mixtures of polymers and charged colloidal spheres or anisotropic colloidal particles and to other inhomogeneous situations. Phase diagrams for mixtures of colloidal rods and nonadsorbing polymer will be presented elsewhere [36]. The free gas-liquid interface and its interfacial

tension of the AO model was recently studied in Ref. [17] by simulations using techniques discussed here.

ACKNOWLEDGMENTS

It is a pleasure to thank R. Evans and J. Brader for stimulating discussions. This work is part of the Research program of the “Stichting voor Fundamenteel Onderzoek der Materie” (FOM), which is financially supported by the “Nederlandse Organisatie voor Wetenschappelijk Onderzoek” (NWO).

-
- [1] A. Vrij, *Pure Appl. Chem.* **48**, 471 (1976).
 [2] F. Leal Calderon, J. Bibette, and J. Biais, *Europhys. Lett.* **23**, 653 (1993).
 [3] S. M. Ilett, A. Orrock, W. C. K. Poon, and P. N. Pusey, *Phys. Rev. E* **51**, 1344 (1995).
 [4] E. H. A. de Hoog, W. K. Kegel, A. van Blaaderen, and H. N. W. Lekkerkerker, *Phys. Rev. E* **64**, 021407 (2001).
 [5] N. A. M. Verhaegh, J. S. van Duijneveldt, J. K. G. Dhont, and H. N. W. Lekkerkerker, *Physica A* **230**, 409 (1996).
 [6] I. Bodnar and W. D. Oosterbaan, *J. Chem. Phys.* **106**, 7777 (1997).
 [7] E. J. Meijer and D. Frenkel, *Phys. Rev. Lett.* **67**, 1110 (1991); *J. Chem. Phys.* **100**, 6873 (1994).
 [8] P. G. Bolhuis, A. A. Louis, and J. P. Hansen, *Phys. Rev. Lett.* **89**, 128302 (2002).
 [9] S. Asakura and F. Oosawa, *J. Chem. Phys.* **22**, 1255 (1954); *J. Polym. Sci.* **33**, 183 (1958).
 [10] A. P. Gast, C. K. Hall, and W. B. Russel, *J. Colloid Interface Sci.* **96**, 251 (1983).
 [11] H. N. W. Lekkerkerker, W. C. K. Poon, P. N. Pusey, A. Stroobants, and P. B. Warren, *Europhys. Lett.* **20**, 559 (1992).
 [12] M. Dijkstra, J. M. Brader, and R. Evans, *J. Phys.: Condens. Matter* **11**, 10079 (1999).
 [13] S. M. Oversteegen and R. Roth, *J. Chem. Phys.* **122**, 214502 (2005).
 [14] E. H. A. de Hoog and H. N. W. Lekkerkerker, *J. Phys. Chem. B* **103**, 5274 (1999).
 [15] J. M. Brader and R. Evans, *Europhys. Lett.* **49**, 678 (2000).
 [16] R. L. C. Vink, A. Jusufi, J. Dzubiella, and C. N. Likos, *Phys. Rev. E* **72**, 030401(R) (2005); R. L. C. Vink and M. Schmidt, *ibid.* **71**, 051406 (2005); R. L. C. Vink and J. Horbach, *J. Chem. Phys.* **121**, 3253 (2004).
 [17] A. Fortini, M. Dijkstra, M. Schmidt, and P. P. F. Wessels, *Phys. Rev. E* **71**, 051403 (2005).
 [18] D. G. A. L. Aarts, M. Schmidt, and H. N. W. Lekkerkerker, *Science* **304**, 847 (2004).
 [19] M. Dijkstra, *Phys. Rev. E* **58**, 7523 (1998).
 [20] M. Dijkstra, R. van Roij, and R. Evans, *Phys. Rev. Lett.* **81**, 2268 (1998); **82**, 117 (1999); *Phys. Rev. E* **59**, 5744 (1999).
 [21] M. Dijkstra, *Curr. Opin. Colloid Interface Sci.* **6**, 372 (2001).
 [22] M. Dijkstra and R. van Roij, *Phys. Rev. Lett.* **89**, 208303 (2002).
 [23] M. Dijkstra and R. van Roij, *J. Phys.: Condens. Matter* **17**, S3507 (2005).
 [24] W. C. K. Poon, *J. Phys.: Condens. Matter* **14**, R859 (2002); *Curr. Opin. Colloid Interface Sci.* **3**, 593 (1998).
 [25] J. M. Brader, R. Evans, and M. Schmidt, *Mol. Phys.* **101**, 3349 (2003).
 [26] J. M. Brader, M. Dijkstra, and R. Evans, *Phys. Rev. E* **63**, 041405 (2001).
 [27] N. F. Carnahan and K. E. Starling, *J. Chem. Phys.* **51**, 635 (1969).
 [28] K. R. Hall, *J. Chem. Phys.* **57**, 2252 (1972).
 [29] W. G. Hoover and F. H. Ree, *J. Chem. Phys.* **49**, 3609 (1968).
 [30] M. Schick, in *Liquids at Interfaces*, edited by J. Charvolin *et al.* (Elsevier, New York, 1990).
 [31] M. Dijkstra, R. van Roij, and R. Evans, *Phys. Rev. E* **63**, 051703 (2001).
 [32] J. M. Brader, R. Evans, M. Schmidt, and H. Löwen, *J. Phys.: Condens. Matter* **14**, L1 (2002).
 [33] W. K. Wijting, N. A. M. Besseling, and M. A. Cohen Stuart, *Phys. Rev. Lett.* **90**, 196101 (2003); *J. Phys. Chem. B* **107**, 10565 (2003).
 [34] D. G. A. L. Aarts and H. N. W. Lekkerkerker, *J. Phys.: Condens. Matter* **14**, S4231 (2004).
 [35] D. G. A. L. Aarts, R. P. A. Dullens, H. N. W. Lekkerkerker, D. Bonn, and R. van Roij, *J. Chem. Phys.* **120**, 1973 (2004).
 [36] S. V. Savenko and M. Dijkstra (unpublished).